

Partial Wave Analysis of  $\psi(3686) \rightarrow \psi(3686) K^+ K^-$ 

M. Ablikim<sup>1</sup>, J. Z. Bai<sup>1</sup>, Y. Ban<sup>11</sup>, J. G. Bian<sup>1</sup>, X. Cai<sup>1</sup>, H. F. Chen<sup>16</sup>, H. S. Chen<sup>1</sup>, H. X. Chen<sup>1</sup>, J. C. Chen<sup>1</sup>, Jin Chen<sup>1</sup>, Y. B. Chen<sup>1</sup>, S. P. Cheng<sup>2</sup>, Y. P. Chu<sup>1</sup>, X. Z. Cui<sup>1</sup>, Y. S. Dai<sup>18</sup>, Z. Y. Deng<sup>1</sup>, L. Y. Dong<sup>1a</sup>, Q. F. Dong<sup>14</sup>, S. X. Du<sup>1</sup>, Z. Z. Du<sup>1</sup>, J. Fang<sup>1</sup>, S. S. Fang<sup>2</sup>, C. D. Fu<sup>1</sup>, C. S. Gao<sup>1</sup>, Y. N. Gao<sup>14</sup>, S. D. Gu<sup>1</sup>, Y. T. Gu<sup>4</sup>, Y. N. Guo<sup>1</sup>, Y. Q. Guo<sup>1</sup>, Z. J. Guo<sup>15</sup>, F. A. Harris<sup>15</sup>, K. L. He<sup>1</sup>, M. He<sup>12</sup>, Y. K. Heng<sup>1</sup>, H. M. Hu<sup>1</sup>, T. Hu<sup>1</sup>, G. S. Huang<sup>1b</sup>, X. P. Huang<sup>1</sup>, X. T. Huang<sup>12</sup>, X. B. Ji<sup>1</sup>, X. S. Jiang<sup>1</sup>, J. B. Jiao<sup>12</sup>, D. P. Jin<sup>1</sup>, S. Jin<sup>1</sup>, Yi Jin<sup>1</sup>, Y. F. Lai<sup>1</sup>, G. Li<sup>2</sup>, H. B. Li<sup>1</sup>, H. H. Li<sup>1</sup>, J. Li<sup>1</sup>, R. Y. Li<sup>1</sup>, S. M. Li<sup>1</sup>, W. D. Li<sup>1</sup>, W. G. Li<sup>1</sup>, X. L. Li<sup>18</sup>, X. Q. Li<sup>10</sup>, Y. L. Li<sup>4</sup>, Y. F. Liang<sup>13</sup>, H. B. Liao<sup>6</sup>, C. X. Liu<sup>1</sup>, F. Liu<sup>6</sup>, Fang Liu<sup>16</sup>, H. H. Liu<sup>1</sup>, H. M. Liu<sup>1</sup>, J. Liu<sup>11</sup>, J. B. Liu<sup>1</sup>, J. P. Liu<sup>17</sup>, R. G. Liu<sup>1</sup>, Z. A. Liu<sup>1</sup>, F. Lu<sup>1</sup>, G. R. Lu<sup>5</sup>, H. J. Lu<sup>16</sup>, J. G. Lu<sup>1</sup>, C. L. Luo<sup>9</sup>, F. C. Ma<sup>8</sup>, H. L. Ma<sup>1</sup>, L. L. Ma<sup>1</sup>, Q. M. Ma<sup>1</sup>, X. B. Ma<sup>5</sup>, Z. P. Ma<sup>1</sup>, X. H. Mo<sup>1</sup>, J. Nie<sup>1</sup>, S. L. Olsen<sup>15</sup>, H. P. Peng<sup>16</sup>, N. D. Qi<sup>1</sup>, H. Qi<sup>9</sup>, J. F. Qiu<sup>1</sup>, Z. Y. Ren<sup>1</sup>, G. Rong<sup>1</sup>, L. Y. Shan<sup>1</sup>, L. Shang<sup>1</sup>, D. L. Shen<sup>1</sup>, X. Y. Shen<sup>1</sup>, H. Y. Sheng<sup>1</sup>, F. Shi<sup>1</sup>, X. Shi<sup>1c</sup>, H. S. Sun<sup>1</sup>, J. F. Sun<sup>1</sup>, S. S. Sun<sup>1</sup>, Y. Z. Sun<sup>1</sup>, Z. J. Sun<sup>1</sup>, Z. Q. Tan<sup>4</sup>, X. Tang<sup>1</sup>, Y. R. Tian<sup>14</sup>, G. L. Tong<sup>1</sup>, G. S. Vamer<sup>15</sup>, D. Y. Wang<sup>1</sup>, L. Wang<sup>1</sup>, L. S. Wang<sup>1</sup>, M. Wang<sup>1</sup>, P. Wang<sup>1</sup>, P. L. Wang<sup>1</sup>, W. F. Wang<sup>1d</sup>, Y. F. Wang<sup>1</sup>, Z. Wang<sup>1</sup>, Z. Y. Wang<sup>1</sup>, Zhe Wang<sup>1</sup>, Zheng Wang<sup>2</sup>, C. L. Wei<sup>1</sup>, D. H. Wei<sup>1</sup>, N. Wu<sup>1</sup>, X. M. Xia<sup>1</sup>, X. X. Xie<sup>1</sup>, B. Xin<sup>8b</sup>, G. F. Xu<sup>1</sup>, Y. Xu<sup>10</sup>, M. L. Yan<sup>16</sup>, F. Yang<sup>10</sup>, H. X. Yang<sup>1</sup>, J. Yang<sup>16</sup>, Y. X. Yang<sup>3</sup>, M. H. Ye<sup>2</sup>, Y. X. Ye<sup>16</sup>, Z. Y. Yi<sup>1</sup>, G. W. Yu<sup>1</sup>, C. Z. Yuan<sup>1</sup>, J. M. Yuan<sup>1</sup>, Y. Yuan<sup>1</sup>, S. L. Zang<sup>1</sup>, Y. Zeng<sup>7</sup>, Yu Zeng<sup>1</sup>, B. X. Zhang<sup>1</sup>, B. Y. Zhang<sup>1</sup>, C. C. Zhang<sup>1</sup>, D. H. Zhang<sup>1</sup>, H. Y. Zhang<sup>1</sup>, J. W. Zhang<sup>1</sup>, J. Y. Zhang<sup>1</sup>, Q. J. Zhang<sup>1</sup>, X. M. Zhang<sup>1</sup>, X. Y. Zhang<sup>12</sup>, Y. Yun Zhang<sup>13</sup>, Z. P. Zhang<sup>16</sup>, Z. Q. Zhang<sup>5</sup>, D. X. Zhao<sup>1</sup>, J. W. Zhao<sup>1</sup>, M. G. Zhao<sup>10</sup>, P. P. Zhao<sup>1</sup>, W. R. Zhao<sup>1</sup>, Z. G. Zhao<sup>1e</sup>, H. Q. Zheng<sup>11</sup>, J. P. Zheng<sup>1</sup>, Z. P. Zheng<sup>1</sup>, L. Zhou<sup>1</sup>, N. F. Zhou<sup>1</sup>, K. J. Zhu<sup>1</sup>, Q. M. Zhu<sup>1</sup>, Y. C. Zhu<sup>1</sup>, Y. S. Zhu<sup>1</sup>, Yingchun Zhu<sup>1f</sup>, Z. A. Zhu<sup>1</sup>, B. A. Zhuang<sup>1</sup>, X. A. Zhuang<sup>1</sup>, B. S. Zou<sup>1</sup>.

(BES Collaboration)

<sup>1</sup> Institute of High Energy Physics, Beijing 100049, People's Republic of China<sup>2</sup> China Center of Advanced Science and Technology, Beijing 100080, People's Republic of China<sup>3</sup> Guangxi Normal University, Guilin 541004, People's Republic of China<sup>4</sup> Guangxi University, Nanning 530004, People's Republic of China<sup>5</sup> Henan Normal University, Xinxiang 453002, People's Republic of China<sup>6</sup> Huazhong Normal University, Wuhan 430079, People's Republic of China<sup>7</sup> Hunan University, Changsha 410082, People's Republic of China<sup>8</sup> Liaoning University, Shenyang 110036, People's Republic of China<sup>9</sup> Nanjing Normal University, Nanjing 210097, People's Republic of China<sup>10</sup> Nankai University, Tianjin 300071, People's Republic of China<sup>11</sup> Peking University, Beijing 100871, People's Republic of China<sup>12</sup> Shandong University, Jinan 250100, People's Republic of China<sup>13</sup> Sichuan University, Chengdu 610064, People's Republic of China<sup>14</sup> Tsinghua University, Beijing 100084, People's Republic of China<sup>15</sup> University of Hawaii, Honolulu, HI 96822, USA<sup>16</sup> University of Science and Technology of China, Hefei 230026, People's Republic of China<sup>17</sup> Wuhan University, Wuhan 430072, People's Republic of China<sup>18</sup> Zhejiang University, Hangzhou 310028, People's Republic of China<sup>a</sup> Current address: Iowa State University, Ames, IA 50011-3160, USA<sup>b</sup> Current address: Purdue University, West Lafayette, IN 47907, USA<sup>c</sup> Current address: Cornell University, Ithaca, NY 14853, USA<sup>d</sup> Current address: Laboratoire de l'Accélérateur Linéaire, F-91898 Orsay, France<sup>e</sup> Current address: University of Michigan, Ann Arbor, MI 48109, USA<sup>f</sup> Current address: DESY, D-22607, Hamburg, Germany

A partial wave analysis of  $\psi(3686) \rightarrow \psi(3686) K^+ K^-$  in  $(2S) \rightarrow \psi(3686)$  decay is presented using a sample of 14 million  $(2S)$  events accumulated by the BES II detector. The data are fitted to the sum of relativistic covariant tensor amplitudes for intermediate resonant decay modes. From the fit, significant contributions to  $\psi(3686)$  decays from the channels  $f_0(980)f_0(980)$ ,  $f_0(980)f_0(2200)$ ,  $f_0(1370)f_0(1710)$ ,  $K(892)^0 K(892)^0$ ,  $K_0(1430)K_0(1430)$ ,  $K_0(1430)K_2(1430) + c.c.$ , and  $K_1(1270)K$  are found. Flavor-SU(3)-violating  $K_1(1270) \rightarrow K_1(1400)$  asymmetry is observed. Values obtained for the masses and widths of the resonances  $f_0(1710)$ ,  $f_0(2200)$ ,  $f_0(1370)$ , and  $K_0(1430)$  are presented.

PACS numbers: 13.25.Gv, 12.38.Qk, 14.40.Gx

## I. INTRODUCTION

Exclusive heavy quarkonium decays constitute an important laboratory for investigating perturbative QCD. Compared to  $J/\psi$  decays, relatively little is known concerning  $\psi_{cJ}$  ( $J = 0; 1; 2$ ) decays [1]. More experimental data on exclusive decays of P-wave charmonia are important for a better understanding of the nature of  $\psi_{cJ}$  states, as well as testing QCD based calculations. Further, the decays of  $\psi_{cJ}$ , in particular  $\psi_{c0}$  and  $\psi_{c2}$ , provide a direct window on glueball dynamics in the  $0^{++}$  and  $2^{++}$  channels, as the  $\psi_{cJ}$  hadronic decays may proceed via  $c\bar{c} \rightarrow gg \rightarrow q\bar{q}q\bar{q}$  [2].

Amplitude analysis of  $\psi_{cJ}$  decays is an excellent tool for studying charmonium decay dynamics. Knowledge of the quantum mechanical decay amplitude allows one to investigate not only the intermediate resonant decay modes but also to properly account for the interference effects between different resonances.

In this paper, partial wave analysis results of  $\psi_{c0} \rightarrow \pi^+ K^+ K^-$  in  $(2S)$   $\psi_{c0}$  decays using 14 million  $(2S)$  events accumulated at the BES II detector are presented. In previous studies of this channel, only the decay modes  $\psi_{c0} \rightarrow K^+ K^- (892)^0 \rightarrow \pi^+ \pi^-$  and  $K^- (892)^0 K^+ (892)^0$  were measured [3, 4]. Here additional information from partial wave analysis is very important.

## II. BES DETECTOR

BES II is a large solid-angle magnetic spectrometer that is described in detail in Ref. [5]. Charged particle momenta are determined with a resolution of  $\frac{\Delta p}{p} = \frac{1}{1 + p^2}$  ( $p$  in GeV/c) in a 40-layer cylindrical drift chamber. Particle identification (PID) is accomplished by specific ionization ( $dE/dx$ ) measurements in the drift chamber and time-of-flight (TOF) measurements in a barrel-like array of 48 scintillation counters. The  $dE/dx$  resolution is  $\frac{\Delta(dE/dx)}{dE/dx} = 8.0\%$ ; the TOF resolution is  $\Delta_{TOF} = 180$  ps for Bhabha events. Outside of the TOF system is a 12 radiation length lead-gas barrel shower counter (BSC), operating in self-quenching streamer mode, that measures the positions and energies of electrons and photons over 80% of the total solid angle. The energy resolution is  $\frac{\Delta E}{E} = 22\% = \frac{\Delta p}{p}$  ( $E$  in GeV). Surrounding the BSC is a solenoid magnet that provides a 0.4 T magnetic field in the central tracking region of the detector. Three double-layer muon counters instrument the magnet flux return and serve to identify muons with momentum greater than 0.5 GeV/c. They cover 68% of the total solid angle.

In this analysis, a GEANT3 based Monte Carlo (MC) simulation package (SIMBES) with detailed consideration of detector performance (such as dead electronic channels) is used. The consistency between data and MC has been checked in many high purity physics channels, and the agreement is quite reasonable [6].

## III. EVENT SELECTION

The selection criteria described below are similar to those used in previous BES analyses [4, 7].

### A. Photon identification

A neutral cluster is considered to be a photon candidate when the angle between the nearest charged track and the cluster is greater than  $15^\circ$ , the first hit is in the beginning six radiation lengths, and the difference between the angle of the cluster development direction in the BSC and the photon emission direction is less than  $30^\circ$ . The photon candidate with the largest energy deposit in the BSC is treated as the photon radiated from the  $(2S)$  and used in a four-constraint (4-C) kinematic fit to the hypothesis  $(2S) \rightarrow \pi^+ K^+ K^-$ .

### B. Charged particle identification

Each charged track, reconstructed using MDC information, is required to be well fit to a three-dimensional helix, be in the polar angle region  $|\cos \theta_{MDC}| < 0.80$ , and have the point of closest approach of the track to the beam axis be within 2 cm of the beam axis and within 20 cm from the center of the interaction region along the beam line. For each track, the TOF and  $dE/dx$  measurements are used to calculate  $\chi^2$  values and the corresponding confidence levels for the hypotheses that the particle is a pion, kaon, or proton.

### C . Event selection criteria

Candidate events are required to satisfy the following selection criteria:

- (1) The number of charged tracks is required to be four with net charge zero.
- (2) The sum of the momenta of the two lowest momentum tracks with opposite charges is required to be greater than  $650 \text{ MeV}/c$ ; this removes contamination from  $(2S) \rightarrow \pi^+ \pi^- J/\psi$  events.
- (3) The confidence level for the 4-C kinematic fit to the decay hypothesis  $(2S) \rightarrow \pi^+ \pi^- K^+ K^-$  is required to be greater than 0.01.

The combined confidence level determined from the 4-C kinematic fit and PID information is used to separate  $\pi^+ \pi^-$ ,  $K^+ K^-$ ,  $K^+ K^- K^+ K^-$ , and the different possible particle assignments for the  $\pi^+ \pi^- K^+ K^-$  final states. This combined confidence level is defined as

$$Z = \frac{1}{\sum_{all}^2} \int f(z; ndf_{all}) dz;$$

where  $f(z; ndf_{all})$  is the  $\chi^2$  probability density function,  $\sum_{all}^2$  is the sum of the  $\chi^2$  values from the 4-C kinematic fit and those of the four track PID assignments, and  $ndf_{all}$  is the corresponding total number of degrees of freedom. For an event to be selected, the combined confidence level of  $\pi^+ \pi^- K^+ K^-$  must be larger than those of the other possibilities. In addition, the PID confidence level of each charged track must be  $> 0.01$ .

Further rejection against  $K_S^0 \rightarrow \pi^+ \pi^-$  is obtained by requiring that any  $\pi^+ \pi^- K^+ K^-$  combination with  $M_{\pi^+ \pi^-}$  in the interval  $(497 \pm 50) \text{ MeV}/c^2$  should have  $r_{xy} < 5 \text{ mm}$ , where  $r_{xy}$  is the distance from the beam axis to the  $\pi^+ \pi^-$  vertex.

The invariant mass distribution for the  $\pi^+ \pi^- K^+ K^-$  events that survive all the above selection requirements is shown in Fig. 1. There are clear peaks corresponding to the  $c_0$  states. The highest mass peak corresponds to  $(2S)$  decays to four charged track final states that are kinematically fitted with an unassociated, low energy photon.

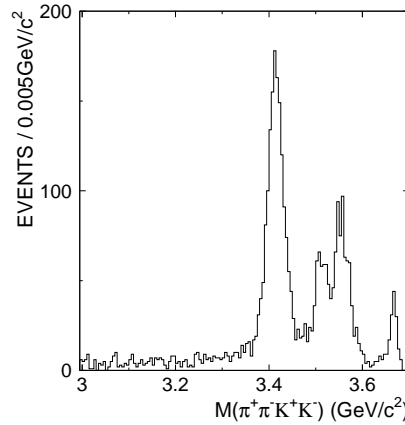


FIG. 1: The  $\pi^+ \pi^- K^+ K^-$  invariant mass spectrum. There are three clear  $c_0$  peaks. The highest mass peak corresponds to  $(2S)$  decays to four charged track final states that are kinematically fitted with an unassociated, low energy photon.

An additional  $\pi^+ \pi^-$  constraint (5-C) kinematic fit is made with the invariant mass of the  $\pi^+ \pi^- K^+ K^-$  being constrained to the  $c_0$  mass. After requiring the confidence level for the 5-C fit to be greater than 0.01, the  $\pi^+ \pi^- K^+ K^-$  invariant mass distributions for data and MC, shown in Fig. 2, are obtained, where the  $\pi^+ \pi^- K^+ K^-$  invariant mass obtained from the 4-C fit and the generated mass and width of the  $c_0$  are fixed to PDG values [1]. The agreement found in this comparison indicates a clean data sample suitable for partial wave analysis in which the four-momentum information from the 5-C fit will be used. Finally, 1371  $(2S) \rightarrow \pi^+ \pi^- c_0$ ;  $c_0 \rightarrow \pi^+ \pi^- K^+ K^-$  candidate events are selected after all the above criteria.

Figure 3 shows the individual  $K^+ K^-$ ,  $\pi^+ \pi^-$ ,  $K^+ K^- \pi^+ \pi^-$ , and  $K^+ K^- K^+ K^-$  invariant mass distributions. There are two strong symmetric structures at about  $1.75 \text{ GeV}/c^2$  and  $2.2 \text{ GeV}/c^2$  and some evidence for  $f_0(980)$  in the  $K^+ K^-$  mass distribution, and there are clear  $(770)$  and  $f_0(980)$  peaks and a smaller one at about  $1.3 \text{ GeV}/c^2$  in the  $\pi^+ \pi^-$  mass distribution. There is no obvious structure for the  $K^+ K^-$  mass spectrum in Fig. 3.

Fig. 4(a) shows the scatter plot of  $K^+ K^-$  versus  $\pi^+ \pi^-$  invariant mass for selected  $(2S) \rightarrow \pi^+ \pi^- c_0$ ;  $c_0 \rightarrow \pi^+ \pi^- K^+ K^-$  events, which provides further information on the intermediate resonant decay modes for  $(\pi^+ \pi^-)(K^+ K^-)$  decay. For instance, it can be seen that the  $f_0(980) \rightarrow \pi^+ \pi^-$  mainly couples with  $f_0(980)$ ;  $f_0(1710)$ ,

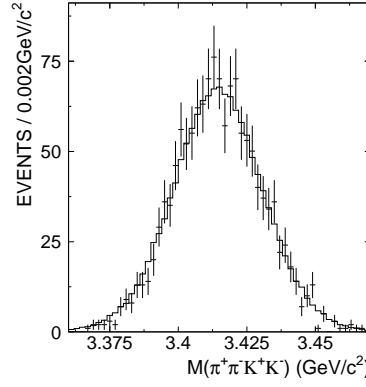


FIG. 2:  $\pi^+\pi^-K^+K^-$  invariant mass distributions from the 4-Cut after requiring  $\text{Prob}_{5C} > 0.01$ , where the error points are data and the histogram is MC.

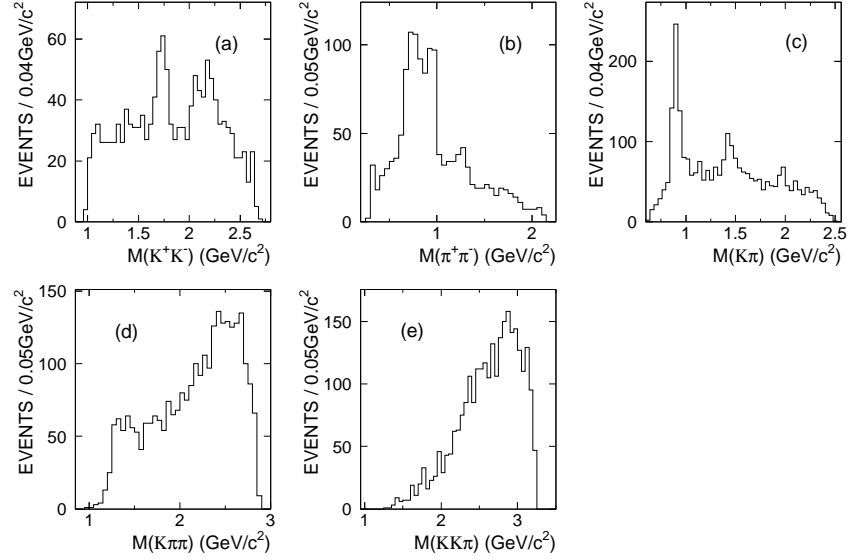


FIG. 3: The individual (a)  $K^+K^-$ , (b)  $\pi^+\pi^-$ , (c)  $K\pi$ , (d)  $K\pi\pi$ , and (e)  $KK\pi$  invariant mass distributions after application of all selection criteria.

and  $f_0(2200)$ , which decay to  $K^+K^-$ , and the concentration of events at large  $K^+K^-$  mass is also associated with  $(770)$  decays to  $\pi^+\pi^-$ .

Figure 4 (b) shows the scatter plot of  $K^+\pi^-$  versus  $K^-\pi^+$  invariant masses. There are obvious clusters due to  $K^*(892)^0$  and around  $1.43 \text{ GeV}/c^2$ , where there are several known resonances, and evidence for  $(K^*)$  structures at about  $1.7 \text{ GeV}/c^2$  and  $1.95 \text{ GeV}/c^2$ , as well as an enhancement above  $2 \text{ GeV}/c^2$ . There is also a possible small accumulation outside the  $K^*(892)^0K^*(892)^0$  cluster, which may be due to the broad S-wave structure.

The  $K$  mass distributions for events where one  $K$  combination is in the  $K^*(892)$  mass region  $896 \pm 60 \text{ MeV}/c^2$  and where the  $\pi^+\pi^-$  mass in the  $(770)$  mass range from  $700$  to  $850 \text{ MeV}/c^2$  are shown in Fig. 5. Strong  $K_1(1270)$  signals are observed in both cases, and there is also a weak peak around  $1.4 \text{ GeV}/c^2$  for the  $K$  decay mode.

Small backgrounds remaining arise mainly from  $(2S)^0 \rightarrow \pi^0 + K^+K^-$ ,  $(2S)^0 \rightarrow \pi^0 + \pi^+\pi^-$ ,  $(2S)^0 \rightarrow \pi^0 + \pi^0\pi^0$ ,  $(2S)^0 \rightarrow \pi^0 + \pi^0\pi^0$ ,  $(2S)^0 \rightarrow \pi^0 + \pi^0\pi^0$ ,  $(2S)^0 \rightarrow \pi^0 + \pi^0\pi^0$ , and  $(2S)^0 \rightarrow \pi^0 + \pi^0\pi^0$ . The number of background events is estimated to be about 29, only a few percent, from detailed exclusive and inclusive MC simulations, and therefore the effect of background is expected to be minor in the following partial wave analysis.

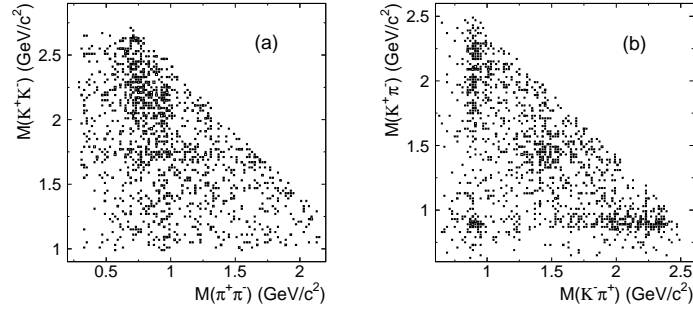


FIG. 4: The scatter plots of (a)  $K^+K^-$  versus  $\pi^+K^-$  and (b)  $K^+\pi^-$  versus  $K^+K^-$  invariant mass for selected  $(2S)$   $\Lambda_c^0$ ;  $\Lambda_c^0 \rightarrow \pi^+K^+K^-$  events.

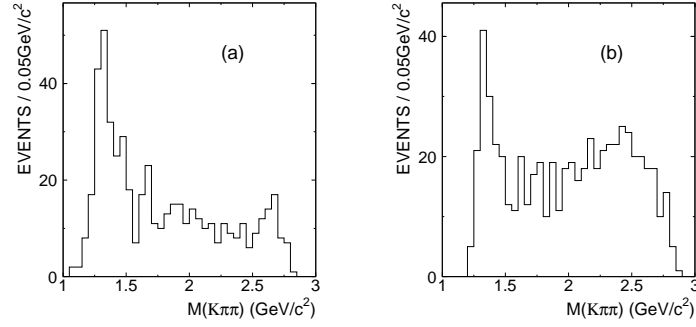


FIG. 5:  $K^+K^-$  invariant mass distributions for events where (a) one  $K^+K^-$  combination is in the mass region  $896 - 960 \text{ MeV}/c^2$  and (b) the  $\pi^+K^-$  invariant mass is in the range  $700 - 850 \text{ MeV}/c^2$ .

#### IV. ANALYSIS RESULTS

We have carried out a partial wave analysis using relativistic covariant tensor amplitudes constructed from Lorentz-invariant combinations of the four-vectors and the photon polarization for  $(2S)$  initial states with helicity  $\pm 1$  [8, 9]. The fit follows the standard isobar model, where each amplitude is assigned a complex coupling constant; the phases associated with these coupling constants originate from final-state interactions. For an intermediate resonance in this analysis, the corresponding Breit-Wigner propagator is denoted by a function:

$$BW = \frac{1}{M^2 - s - iM\Gamma};$$

where  $s$  is the invariant mass-squared and  $M, \Gamma$  are the resonance mass and width. Angular momenta  $L$  up to 2 in the production process are needed, but higher  $L$  give negligible contributions. Standard Blatt-Weisskopf centrifugal barrier factors [8, 9] are included using a radius of interaction of  $0.8 \text{ fm}$ , though results are insensitive to this radius.

The relative magnitudes and phases of the amplitudes are determined by a maximum likelihood fit. The probability density function  $f(\mathbf{x}_i; \mathbf{p})$  with  $\mathbf{x}_i$  as a set of independently measured quantities and  $\mathbf{p}$  as a set of unknown parameters is defined as:

$$f(\mathbf{x}_i; \mathbf{p}) = \frac{d}{d\mathbf{p}} = ;$$

where the differential cross section is given by

$$\frac{d}{d\mathbf{p}} = \frac{1}{jA_{\text{total}}} \frac{d}{d\mathbf{p}} = \sum_{i=1}^X A_i \frac{d}{d\mathbf{p}} :$$

Here,  $A_i$  is the relativistic covariant tensor amplitude. The total cross section  $\sigma = \int \frac{d}{d\mathbf{p}} d\mathbf{p} = \sum_{i=1}^{N_{MC}} jA_{\text{total}} \frac{d}{d\mathbf{p}}$  is calculated using a MC integration, where  $N_{MC}$  is the number of simulated MC events. A fit is made to the data in

order to maximize the value of

$$L = \prod_{i=1}^{N_{\text{event}}} f(\mathbf{x}_i; \boldsymbol{\theta}):$$

Actually,  $S = -\ln L$  is minimized in the fit.

Background events obtained from MC simulation are included in the fit, but with the opposite sign of log likelihood compared to data. These events are used to cancel the backgrounds within the data sample in the maximum likelihood fit.

Table I shows the decay modes considered in the partial wave analysis, which are motivated by the structures seen in the scatter plots of Figs. 4(a) and (b) and in projections of Figs. 3 and 5, and changes  $S$  in log likelihood when the component is dropped from the fit. The partial wave amplitude improves log likelihood by more than 5 in most cases. The decay modes  $f_0(980)f_0(1710)$ ,  $f_2(1270)f_2(1270)$ , and  $f_0(1710)f_0(1370)$ , where for the latter  $f_0(1710)$  decays to  $\pi^+\pi^-$  and  $f_0(1370)$  decays to  $K^+K^-$ , are shown for completeness, but they are not very significant. The mass projections in  $K^+K^-$ ;  $\pi^+\pi^-$ ;  $K^+K^-$ , and  $K^+K^-$  are shown in Fig. 6. There is a reasonable agreement between the data and the fit.

TABLE I: Decay modes fitted in the partial wave analysis and changes  $S$  in log likelihood when the component is dropped from the fit.

Decay mode	Fitted events	$S$
$(\pi^+\pi^-)(K^+K^-)$		
$f_0(980)f_0(980)$	27.9	15.7
$f_0(980)f_0(1710)$	14.7	5.2
$f_0(980)f_0(2200)$	77.1	27.3
$f_0(1370)f_0(980)$	26.9	14.6
$f_0(1370)f_0(1710)$	60.6	23.5
$f_2(1270)f_2(1270)$	5.9	5.8
$f_0(1710)$	46.7	22.2
$f_0(2200)$	23.9	8.5
$f_0(1710)f_0(1370)$	4.6	2.5
$(K^+\pi^-)(K^-\pi^+)$		
$K^-(892)^0 K^+(892)^0$	64.5	31.1
$K^-(892)^0 K^+(1680)^0 + \text{c.c.}$	40.5	21.0
$K_0^-(1430) K_0^+(1430)$	82.9	28.0
$K_2^-(1430) K_2^+(1430)$	9.2	7.1
$K_0^-(1430) K_2^+(1430) + \text{c.c.}$	62.0	40.6
$K_0^-(1430) K_0^+(1950) + \text{c.c.}$	71.0	22.7
	106.8	39.2
$K^-(892)^0 K^+(2300)^0 + \text{c.c.}$	115.7	45.2
$(K^+\pi^-)K^-$		
$K_1^-(1270)^+ K^- + \text{c.c.}$	153.0	102.2
$K_1^-(1400)^+ K^- + \text{c.c.}$	19.7	6.9
$K^-(1460)^+ K^- + \text{c.c.}$	79.7	39.3

$$A_{\pi^+\pi^-} = c_0 |(\pi^+\pi^-)(K^+K^-)|$$

We begin by discussing the  $c_0 |(\pi^+\pi^-)(K^+K^-)|$  decay modes. In Fig. 6(b), the  $\pi^+\pi^-$  due to the decay of  $K_1^-(1270)^+ K^-$  and a strong  $f_0(980)$  are observed. Along the  $f_0(980)$  ( $\pi^+\pi^-$ ) band in Fig. 4(a), there are several enhancements, one at the  $K^+K^-$  threshold and others around  $1.75 \text{ GeV}/c^2$  and  $2.2 \text{ GeV}/c^2$ , which correspond to the  $f_0(980)f_0(980)$ ;  $f_0(980)f_0(1710)$ , and  $f_0(980)f_0(2200)$  modes listed in Table I.

In the fit, the  $f_0(980)$  is described with the usual Flatté formula [10, 11], and the parameters used are those of Ref. [11]. At higher  $\pi^+\pi^-$  mass, a weak signal around  $1.3 \text{ GeV}/c^2$  is visible. It is mainly from couplings of the  $f_0(1370)$  with  $f_0(980)$  and  $f_0(1710)$  which decay to  $K^+K^-$ . A fit to  $f_0(1370)$  gives a fitted mass of  $1265 \pm 30 \text{ MeV}/c^2$  and a width of  $350 \pm 100 \text{ MeV}/c^2$  with large statistical errors. Apart from the above structures, a correlation between the low  $\pi^+\pi^-$  mass enhancement and  $K^+K^-$  mass greater than  $1.5 \text{ GeV}/c^2$  also appears in Fig. 4(a). We describe it by adding  $f_0(1710)$  and  $f_0(2200)$  decay modes, where the parameterization of a  $J = 0 \rightarrow 0 \rightarrow \pi^+\pi^-$  analysis

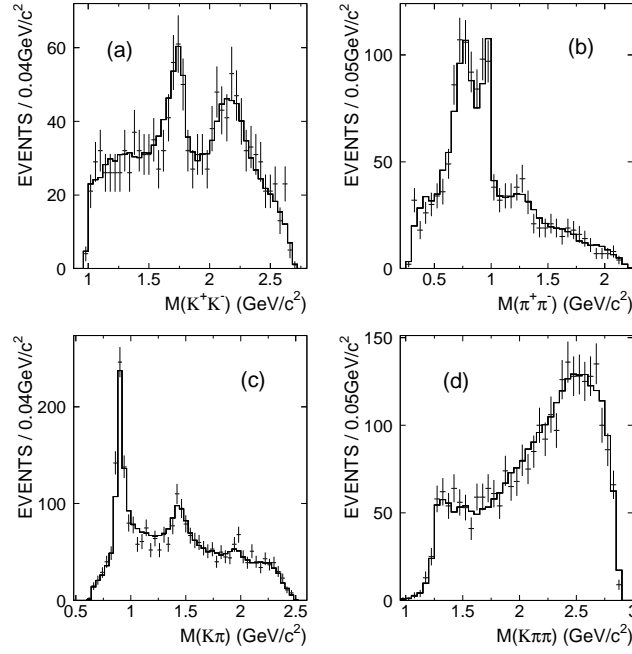


FIG. 6: Mass projections on (a)  $K^+K^-$ , (b)  $\pi^+\pi^-$ , (c)  $K\pi$  and (d)  $K\pi\pi$  for  $(2S) \rightarrow c_0; c_0 \rightarrow \pi^+ K^+ K^-$ . The histograms represent the fit result, and the points with error bars are data.

(Adler zero parameterization) [12] is adopted to describe the broad S-wave. The  $f_0(1710)$  and  $f_0(1370)f_0(1710)$  decays dominate the production of  $f_0(1710)$  in the partial wave of  $(2S) \rightarrow c_0; c_0 \rightarrow \pi^+ K^+ K^-$ .

The fitted mass and width of the  $f_0(1710)$  are  $M = 1760 \pm 15 \text{ MeV}/c^2$  and  $\Gamma = 125 \pm 25 \text{ MeV}/c^2$ . The mass is somewhat higher than the PDG value [1]. The  $f_0(1790)$  has been recently claimed in  $J =$  decays [13]. The parameters of  $f_0(1790)$  and those of  $f_0(1710)$  given by the PDG and Ref. [14] are tested in this analysis, and the log likelihood becomes worse by 10.3, 11.5, and 4.2, respectively. The log likelihood can be improved by 5.7 if both the  $f_0(1790)$  and  $f_0(1710)$  (using parameters of Ref. [14]) are included into the fit, while the results for the other components only change a little. A fit replacing the decay modes with an  $f_0(1710)$  with  $f_2(1710)$  (namely, using  $f_2(1710); f_0(980)f_2(1710)$ , and  $f_0(1370)f_2(1710)$  decays instead of  $f_0(1710); f_0(980)f_0(1710)$ , and  $f_0(1370)f_0(1710)$  in the fit) is made in order to check the spin-parity of the structure around  $1.75 \text{ GeV}/c^2$  in the  $K^+K^-$  mass region. It gives a worse log likelihood by 55.6 and a poor fit result, as shown in Fig. 7(a).

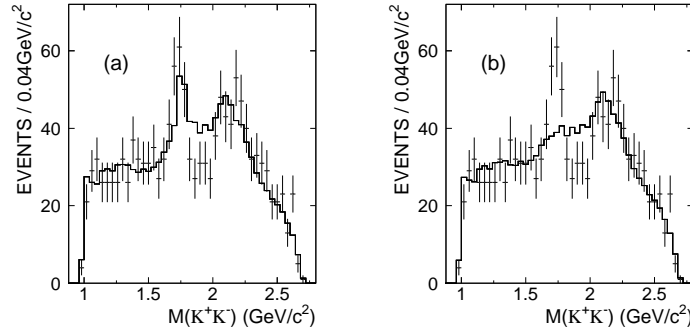


FIG. 7: Mass projections in  $K^+K^-$  for fits replacing  $f_0(1710)$  with (a)  $f_2(1710)$  or (b)  $f(1450)$  and  $f(1700)$ . The dots with error bars are data, and the histograms are the fits.

There are two  $\omega$ -like resonances,  $f(1450)$  and  $f(1700)$ , which decay to  $KK$  final states in the  $1600\text{--}1700 \text{ MeV}/c^2$  region [1]. As a check, we add  $f(770)f(1450)$  and  $f(770)f(1700)$  intermediate decay modes into the fit with four more fitted parameters, using the mass and width measurements given by Ref. [15], and the log likelihood is improved by 6.4. Replacing the components  $f_0(1710)$ ,  $f_0(980)f_0(1710)$ , and  $f_0(1370)f_0(1710)$  with  $f(770)f(1450)$  and  $f(770)f(1700)$  gives a worse log likelihood by 81.6, and the corresponding fit is shown in Fig. 7(b). An investigation of the  $f(770)$



band in Fig. 4 (a) indicates that the structures at high  $K^+K^-$  mass are a reflection of the other intermediate decay modes.

A fit to  $f_0(2200)$  gives a fitted mass of  $2170 \pm 20 \text{ MeV}/c^2$  and a width of  $220 \pm 60 \text{ MeV}/c^2$ . There are several scalar and tensor resonances located in the mass range greater than  $2.0 \text{ GeV}/c^2$  which decay to the  $K^+K^-$  final states [1]:  $\rho(2150)$ ,  $f_2(2150)$ ,  $f_0(2200)$ , and  $f_2(2300)$ . A variety of alternative fits to the high  $K^+K^-$  mass region, listed in Table II, using these resonances and the  $f_0(2100)$  have been tried. Note that PDG mass and width values [1] are used in the fits for the  $f_0(2100)$ ,  $f_2(2150)$ ,  $\rho(2150)$ , and  $f_2(2300)$  and that  $f_0(2100)$ ,  $f_2(2150)$ ,  $f_0(2200)$ , and  $f_2(2300)$  couple with the  $\pi\pi$  and  $f_0(980)$ , while the  $\rho(2150)$  couples with the  $\eta(770)$ . We also tried  $f_2(2200)$  instead of the  $f_0(2200)$  in one fit, assuming it couples with the  $\pi\pi$  and  $f_0(980)$ .

TABLE II: Alternative fits to the high  $K^+K^-$  mass region instead of using only a  $f_0(2200)$  involved in the fit; the right-hand column shows values of  $S$ ; positive values indicate poorer fits.

Components	$S$
a) $\rho(2150)$	+ 35.3
b) $f_2(2200)$ $M = 2170 \text{ MeV}/c^2$ , $\Gamma = 220 \text{ MeV}/c^2$	+ 33.1
c) $f_2(2150) + f_0(2200)$	-4.5
d) $f_2(2150) + f_0(2100)$	+ 9.9
e) $f_2(2150) + f_2(2300)$	+ 28.6
f) $f_0(2100) + f_0(2200)$	-4.3
g) $f_0(2100) + f_2(2300)$	-3.5
h) $f_0(2200) + f_2(2300)$	-9.0
i) $f_2(2150)$	+ 32.5

In Table II, fit a), using  $\eta(770)$   $\rho(2150)$  instead of  $f_2(2200)$  and  $f_0(980)f_0(2200)$ , gives a worse log likelihood by 35.3. A fit with both  $f_0(2200)$  and  $\rho(2150)$  improves the log likelihood by about 3.0 compared to the case with  $f_0(2200)$  only. Also b), e), and i), where no scalar is included, as well as d), give bad fits. Fits c), f), g), and h) improve the log likelihood a little, but not significantly.

Based on these fit results, we conclude that a scalar state  $f_0(2200)$  at about  $2.2 \text{ GeV}/c^2$  which decays to  $K^+K^-$  is needed in this channel, but no additional significant  $0^{++}$  or  $2^{++}$  is required in this mass region according to our study in Table II.

$$B \rightarrow \pi^0 \pi^0 (K^+ K^-) (K^+ K^-)$$

The shape of the  $K^*(892)$  is described by a P-wave relativistic Breit-Wigner curve, with a width

$$\Gamma = \Gamma_0 \frac{m_0}{m} \frac{1 + r^2 p_0^2}{1 + r^2 p^2} \frac{p}{p_0}^3;$$

where  $m$  is the mass of the  $K^*$  system,  $p$  is the momentum of kaon in the  $K^*$  system,  $\Gamma_0$  is the width of the resonance,  $m_0$  is the mass of the resonance,  $p_0$  is  $p$  evaluated at the resonance mass,  $r$  is the interaction radius and  $\frac{1 + r^2 p_0^2}{1 + r^2 p^2}$  represents the contribution of the barrier factor. The value  $(3.4 \pm 0.6 \pm 0.3) (\text{GeV}/c)^{-1}$  measured by the  $K^+K^-$  scattering experiment [16] as an approximate estimation of the interaction radius  $r$  is used.

Adding a  $K^*(892)^0 K^*(1680)^0$  decay mode improves log likelihood by 21.0, where the mass and width of  $K^*(1680)^0$  are fixed to PDG values [1] and the interaction radius  $r$  in the fit is set to the value 2.0 given by Ref. [16].

Most of the peak at  $1430 \text{ MeV}/c^2$  is fitted as  $K_0^*(1430)K_0^*(1430)$  and  $K_0^*(1430)K_2^*(1430)$  events is about 11% of that of  $K_0^*(1430)K_0^*(1430)$ . Adding the  $K_2^*(1430)K_2^*(1430)$  mode improves the log likelihood by 7.1, which corresponds to about a significance of 3.3 for two free parameters of the fitted amplitudes. The mass and width of the  $K_2^*(1430)$  are fixed to the PDG values [1]. A fit to  $K_0^*(1430)$  gives a fitted mass of  $1455 \pm 20 \text{ MeV}/c^2$  and a width of  $270 \pm 45 \text{ MeV}/c^2$ .

There is another structure visible around  $1.95 \text{ GeV}/c^2$  in the  $K^*$  mass distribution. Among the three generalized C-parity allowed intermediate decays from  $\pi^0\pi^0$ ,  $K_0^*(1430)K_0^*(1950)$ ,  $K_2^*(1430)K_0^*(1950)$ , and  $K_0^*(1950)$ , the first decay gives a better log likelihood value in our fit than the other two by 22.9 and 14.6, respectively. A fit gives



assumed mass of  $1945 \pm 30 \text{ MeV}/c^2$ , but the width is poorly determined,  $\sim 500 \text{ MeV}/c^2$ , so we adopt the PDG mass and width values for the  $K_0(1950)$  in the partial wave analysis.

In Fig. 4(b) there is a possible accumulation outside the  $K(892)^0 K(892)^0$  cluster. Its explanation may be the broad S-wave. Since the properties of are still controversial (cf., the review paper in the PDG [1], and references therein), we use a Breit-Wigner amplitude of constant width, without any phase space factor with the parameterization obtained in Ref. [17],  $M = 790 \text{ MeV}/c^2$ ,  $\Gamma = 860 \text{ MeV}/c^2$  to describe this broad structure. The log likelihood becomes worse by 39.2 after removing the from the fit, and the corresponding projection in  $K$  mass, shown in Fig. 8, obviously disagrees with data at low  $K$  mass.

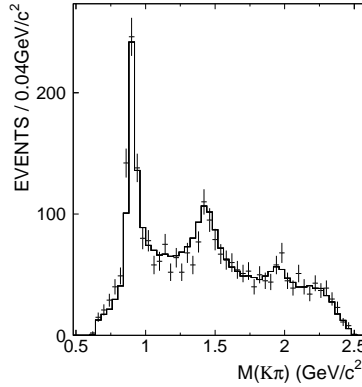


FIG. 8: The  $K$  mass projection for the fit without decay.

Finally, an intermediate decay mode  $K(892)^0 K(2300)^0$  is added into the fit. Here the  $K(2300)^0$  is used as an effective structure to describe the poorly known high  $K$  mass region. The log likelihood changes by 45.2 if the  $K(892)^0 K(2300)^0$  is omitted. The scanned mass and width for  $K(2300)^0$  are  $2.3 \text{ GeV}/c^2$  and  $300 \text{ MeV}/c^2$  respectively. No higher spin-parity tests such as 3 or 5 are made.

$$C = c_0 ! (K^+ )K$$

In Fig. 5 there are strong  $K_1(1270)$  signals in both  $K(770)$  and  $K(892)$ , and there is also a weak peak around  $1.4 \text{ GeV}/c^2$  in the  $K(892)$ . In the partial wave analysis,  $K_1(1270)K$  and  $K_1(1400)K$  decays, where  $K_1(1270)$  decays to  $K(770)$ ;  $K(892)$ , and  $K_0(1430)$  and  $K_1(1400)$  decays to  $K(892)$ , are added. The fit also requires an additional structure to describe the  $K$  mass distribution at about  $1.4 \text{ GeV}/c^2$ . Here adding  $K(1460)$  in the fit will improve the log likelihood by 39.3; in the fit, the mass and width values given by the PDG [1] are used. The masses and widths of the  $K_1(1270)$  and  $K_1(1400)$  are also fixed to PDG values so as to reduce uncertainties.

There are two lowest-lying axial-vector meson octets. These correspond to the singlet ( $^1P_1$ ) and triplet ( $^3P_1$ ) spin configurations of two quarks in a P-wave orbital angular momentum state. The nonstrange, isospin  $I = 1$  members of the two octets have opposite G parity: the  $b_1(1235)$  is in the  $^1P_1$  octet and has  $G = +1$ , while the  $a_1(1260)$  is in the  $^3P_1$  octet and has  $G = -1$ . The strange members of the  $^3P_1$  and  $^1P_1$  octets, the  $K_A$  and  $K_B$ , respectively, are mixtures of the observed physical states, the  $K_1(1270)$  and the  $K_1(1400)$ , where

$$K_A = \cos \theta K_1(1400) + \sin \theta K_1(1270);$$

$$K_B = \cos \theta K_1(1270) - \sin \theta K_1(1400);$$

and the mixing angle is near  $\theta \approx 45^\circ$  [18]. The dominant  $K_1(1270)$  decay mode is to  $K(770)$  ( $B = 42\% \pm 6\%$ ); the  $K_1(1400)$  decays almost always to  $K(892)$  ( $B = 94\% \pm 6\%$ ): In the limit of strict flavor SU(3) symmetry, the amplitudes for two-body decays to conjugate mesons in the same pair of octets should be equal. Thus, since decays to  $b_1$  are forbidden by G parity, decays to  $K_B K$  are disallowed by SU(3), and one expects relatively pure  $K_A K$  final states in  $c_0$  decays. And, since  $\theta \approx 45^\circ$ , there should be roughly equal amounts of  $K_1(1270)$  and  $K_1(1400)$ .

The remarkable feature of the  $K$  distribution is that the contribution of the  $K_1(1400)$  in the final fit is very small compared to the large  $K_1(1270)$  signal. Adding a  $K_1(1400)$  improves the log likelihood by 6.9 which corresponds to the significance of about 2.7. The partial wave analysis yields a  $K_1(1270) \rightarrow K(770)$  signal of  $68.3 \pm 11.0$  events and a  $K_1(1400) \rightarrow K(892)$  signal of  $19.7 \pm 6.9$  events. The function used to fit the  $K_1(1270)$  is a convolution of an S-wave Breit-Wigner function for the  $K_1(1270)$  with a P-wave Breit-Wigner function for the  $(770)$  meson. Flavor-SU(3)-violating  $K_1(1270) \rightarrow K_1(1400)$  asymmetry for  $c_0$  decay is observed.

## D . GOODNESS-OF-FIT

To determine the goodness of fit, a  $\chi^2$  is calculated by comparing histograms, e.g.; a vector of Poisson distributed numbers  $n = (n_1; \dots; n_N)$ ; with a hypothesis for their expectation values  $\mu_i = E[n_i]$ . As the distribution is Poisson with variances  $\sigma_i^2 = \mu_i$ , the  $\chi^2$  becomes Pearson's  $\chi^2$  statistic,

$$\chi^2 = \sum_{i=1}^N \frac{(n_i - \mu_i)^2}{\mu_i}.$$

If the hypothesis  $\mu = (\mu_1; \dots; \mu_N)$  is correct and if the measured values  $n_i$  are sufficiently large, then the  $\chi^2$  statistic will follow the  $\chi^2$  probability density function with the number of degrees of freedom (ndf) equal to the number of measurements  $N$  minus the number of fitted parameters.

For an  $n$ -body final state, the number of independent kinematic variables is  $3n - 4$ . Thus, one can compare  $3n - 4$  selected independent variables with the fit results by defining a quantity

$$\chi_{\text{all}}^2 = \sum_{j=1}^{3n-4} \chi_j^2$$

to check the quality of a global fit, which obeys the  $\chi^2$  distribution approximately with the number of degrees of freedom equal to the total number of measurements minus the number of fitted parameters; and the individual  $\chi_j^2$  will give a qualitative measure of the goodness of fit for each kinematic variable.

The number of independent kinematic variables for  $(2S) \rightarrow c_0; c_0 \rightarrow K^+ K^-$  process is 10 after the use of the 5-Cut with the additional  $c_0$  mass constraint. We use the following 10 distributions to check the goodness-of-fit:

- {  $(\theta; \phi)_{KK}$  = the polar angle and azimuthal angle of the  $(K^+ K^-)$  in the laboratory system,
- {  $(\theta; \phi)_K$  = the polar angle and azimuthal angle of the  $(K^+ K^-)$  in the  $(K^+ K^-)$  center of mass,
- {  $(\theta; \phi)_K$  = the polar angle and azimuthal angle of the  $(K^+ K^-)$  in the  $(K^+ K^-)$  center of mass,
- {  $(\theta; \phi) =$  the polar angle and azimuthal angle of the  $K^+$  in the  $(K^+ K^-)$  center of mass,

and the invariant masses for the  $(K^+ K^-)$  and  $(K^+ K^-)$  systems. Table III shows the results, where the number of bins is taken as the number of degrees of freedom for each individual distribution, and Fig. 9 shows the projections of the 10 variables. There is excellent agreement between the data and fit.

TABLE III: Check of goodness of fit using 10 independent kinematic variables, where ndf and C.L. are the number of degrees of freedom and the corresponding confidence level.

Variable	$\chi^2$	ndf	$\chi^2/\text{ndf}$	C.L.
$\cos \theta_{KK}$	24.46	18	1.36	0.14
$\phi_{KK}$	14.23	20	0.71	0.82
$\cos \theta_K$	11.29	20	0.56	0.94
$\phi_K$	22.58	20	1.13	0.31
$\cos \theta_{K^+}$	11.34	16	0.71	0.79
$\phi_{K^+}$	18.81	20	0.94	0.53
$\cos \theta$	12.15	20	0.61	0.91
$\phi$	12.63	20	0.63	0.89
$M_{K^+ K^-}$	37.26	36	1.04	0.41
$M_{K^+ K^-}$	55.07	47	1.17	0.20

Using the results in Table III, the  $\chi_{\text{all}}^2$  obtained is 219.8 with a 185 degrees of freedom ( $= 237 - 52$ , where 237 is a sum of the bin numbers for the 10 distributions and 52 is the number of fitted amplitude parameters), which corresponds to a confidence level of 4%.

## V . SYSTEMATIC ERROR

In this analysis, the systematic errors are estimated by considering the following sources:

- (1) Uncertainty of the parameterization of the line shape: use a Breit-Wigner amplitude of constant width  $M = 470 \text{ MeV}/c^2$ ,  $\Gamma = 613 \text{ MeV}/c^2$  [12] instead of the Adler zero parameterization.

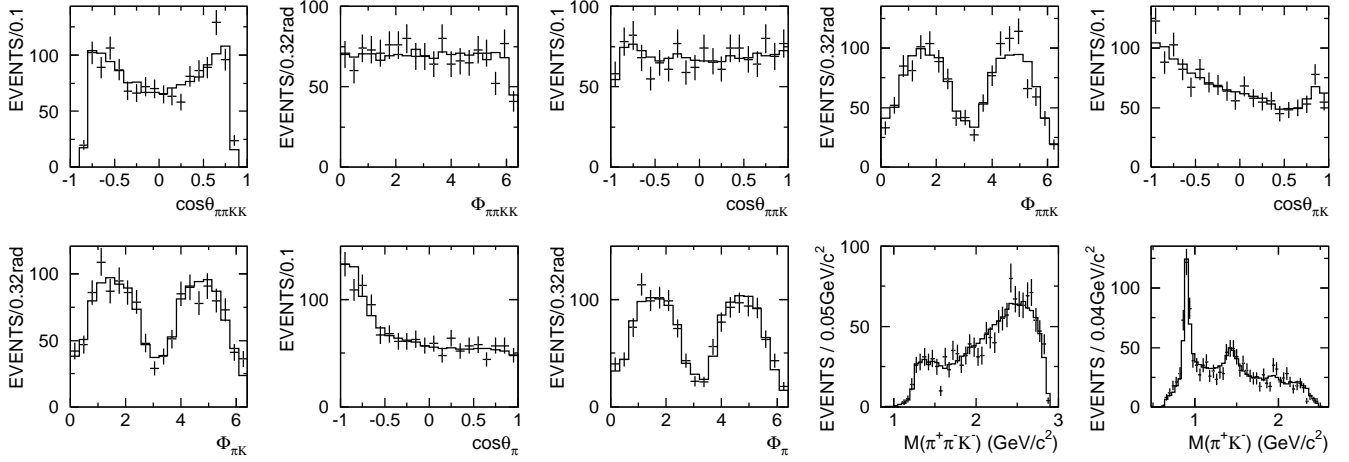


FIG. 9: Fit projections for the 10 variables described in the text after the global  $\chi^2$  fit.

(2) Uncertainty of the parameterization of the  $\pi^+\pi^-K$  line shape: change the mass and width of the Breit-Wigner amplitude of constant width to  $M = 745 \text{ MeV}/c^2$ ,  $\Gamma = 622 \text{ MeV}/c^2$  [17].

(3) The parameters of the  $f_0(980)$  are still uncertain, and in addition to the solution of Ref. [11], we also use measurements of some recent experiments such as E791, GAMOS, and WA102 [19, 20, 21], where a Breit-Wigner description with the width varying from 44 to 80  $\text{MeV}/c^2$  was used for the  $f_0(980)$ . We determine the change both by using the solutions of Refs. [19, 20, 21] and by varying  $g_1$  in Ref. [11] from 0.1108  $\text{GeV}/c^2$  to 0.090  $\text{GeV}/c^2$  and 0.130  $\text{GeV}/c^2$  while keeping the ratio  $g_2=g_1$  fixed.

(4) As mentioned above, we use the measurement of Ref. [16],  $(3.4 \pm 0.6 \pm 0.3) (\text{GeV}/c)^{-1}$  for  $r$  in the P-wave relativistic Breit-Wigner parameterization. We also use  $r$  varied by one sigma to  $2.73 (\text{GeV}/c)^{-1}$  and  $4.07 (\text{GeV}/c)^{-1}$  to determine the change in the  $\chi^2$ .

(5) Vary mass and width values of the  $(K^-)$  components  $K_2(1430)$ ,  $K_1(1680)$ , and  $K_0(1950)$  within the PDG errors [1].

(6) Vary mass and width values of the  $(K^-)$  components  $K_1(1270)$ ,  $K_1(1400)$ , and  $K_1(1460)$  within the PDG errors [1], where the width of  $K_1(1460)$  is changed to 200 and 300  $\text{MeV}/c^2$  and mass to 1.40 and 1.46  $\text{GeV}/c^2$ .

(7) Remove the small component  $f_0(1710)f_0(1370)$  from the  $\chi^2$ , where  $f_0(1710)$  decays to  $\pi^+\pi^-$  and  $f_0(1370)$  decays to  $K^+K^-$ .

(8) Add three  $(K^-)$  resonances  $K_1(1650)$ ,  $K_2(1770)$ , and  $K_2(1820)$  into the  $\chi^2$ .

(9) Remove the  $K(892)^0K(2300)^0 + c.c.$  decay mode from the original  $\chi^2$  but keep (8). Tests (8) and (9) strongly affect the branching fraction measurements.

(10) Try alternative starting conditions for the maximum likelihood  $\chi^2$ .

(11) Uncertainty of the background in the partial wave analysis  $\chi^2$ .

Total errors are obtained by adding the individual errors in quadrature. For the branching fraction uncertainties, the uncertainties in MDC tracking, kinematic fitting, PID, efficiency of the photon ID, and the number of (2S) events [22] are also included, and the total systematic error for this part, 12%, is taken from Ref. [4].

## VI. DISCUSSION

From the  $\phi \rightarrow \pi^+ K^+ K^-$  decay fit results, it is found that scalar resonances have large decay fractions compared to those of tensors, and such decays provide a relatively clean laboratory in which to study the properties of the scalars  $f_0(980)$ ,  $f_0(1370)$ ,  $f_0(1710)$ , and  $f_0(2200)$ . There is conspicuous production due to the  $K(892)^0K(892)^0$  and  $K_0(1430)K_0(1430)$  (and  $K_0(1430)K_2(1430) + c.c.$ ) pairs, and Flavor-SU(3)-violating  $K_1(1270) \rightarrow K_1(1400)$  asymmetry is observed. Information on these states is very desirable and will be described below.

For other components in Table I, because of the low statistics ( $f_2(1270)f_2(1270)$ ,  $f_0(1710)f_0(1370)$ , and  $K_2(1430)K_2(1430)$ ), uncertain parameters of intermediate resonances involved ( $f_0(1710)$ ,  $f_0(2200)$ ,  $K(892)^0K(1680)^0 + c.c.$ ,  $K_0(1430)K_0(1950) + c.c.$ , and  $K(1460)K^-$ ), and the poorly known high mass  $K^-$  region which is described by the  $K(892)^0K(2300)^0 + c.c.$ , it is difficult to obtain precise quantitative results or make definite conclusions. The systematic errors on the numbers of events for decay modes  $f_0(980)f_0(1710)$  and

$f_0(1370)f_0(980)$  are very large, while the significance of the  $f_0(980)f_0(1710)$  is small; therefore we also will not consider these two decay modes in the following branching fraction measurements.

The numbers used in the branching fraction (or upper limit) calculations and the corresponding results are summarized in Table IV, where the first errors are statistical and the second are systematic. The value of  $B[(2S) \rightarrow c_0 \rightarrow \pi^+ K^+ K^-]$ , (9.22  $\pm$  0.11  $\pm$  0.46)%; recently measured by the CLEO experiment, is used [23]. The term moving the  $K_1(1270) \rightarrow K(770)$  gives a worse log likelihood by 39.5, which corresponds to the signal significance of about 8.6. The 90% confidence level (C.L.) upper limit for  $c_0 \rightarrow K_1(1400)K$  is obtained by increasing the number of events by 1.28, where includes the statistical and the systematic errors added in quadrature.

TABLE IV: Summary of numbers used in the branching fraction (or upper limit) calculations and corresponding results, where  $X$  represents the intermediate decay modes,  $N^{fit}$  is the number of fitted events, and  $\epsilon$  is the efficiency.

Decay mode	$N^{fit}$			(%)	Sys. error (%)	$B[c_0 \rightarrow X \rightarrow \pi^+ K^+ K^-]$	$(10^{-4})$		Significance
$f_0(980)f_0(980)$	27.9	6.7	6.25	0.01	$+55.7^{+45.3}_{-19.6}$	3.46	$0.83^{+1.93}_{-1.57}$		5.3
$f_0(980)f_0(2200)$	77.1	10.6	7.09	0.01	$+19.6^{+27.2}_{-46.1}$	8.42	$1.16^{+1.65}_{-2.29}$		7.1
$f_0(1370)f_0(1710)$	60.6	12.4	6.59	0.01	$+27.2^{+23.6}_{-28.3}$	7.12	$1.46^{+3.28}_{-1.68}$		6.5
$K^-(892)^0 K^+(892)^0$	64.5	9.9	6.18	0.01	$+46.1^{+23.6}_{-28.3}$	8.09	$1.24^{+2.29}_{-1.99}$		7.1
$K_0^-(1430)K_0^+(1430)$	82.9	12.5	6.15	0.01	$+29.2^{+24.6}_{-18.2}$	10.44	$1.57^{+3.05}_{-1.90}$		7.2
$K_0^-(1430)K_2^+(1430) + c.c.$	62.0	10.7	5.66	0.01	$+18.2^{+15.6}_{-23.4}$	8.49	$1.47^{+1.99}_{-1.99}$		8.7
$K_1(1270)^+ K^- + c.c.$									
$K_1(1270) \rightarrow K^-(770)$	68.3	11.0	5.68	0.01	$+19.4^{+17.6}_{-17.6}$	9.32	$1.50^{+1.81}_{-1.64}$		8.6
$K_1(1400)^+ K^- + c.c.$									
$K_1(1400) \rightarrow K^-(892)$	19.7	6.9	4.94	0.01	$+21.9^{+24.5}_{-24.5}$	< 11.9 (90% C.L.)			2.7

The partial wave fit provides magnitudes and phases of the different partial amplitudes, as well as the interference terms. The intensity from these amplitudes is used to weight both the complete set of generated MC events and the set which survives the selection procedure. The ratio between these two weighted sets is the efficiency.

Using the number of selected  $(2S) \rightarrow c_0 \rightarrow \pi^+ K^+ K^-$  events, the overall efficiency determined by the method above, (5.85  $\pm$  0.01)%, and the result of Ref. [23] we get the corresponding branching fractions after subtracting background

$$B[(2S) \rightarrow c_0 \rightarrow \pi^+ K^+ K^-] = (1.64 \pm 0.05 \pm 0.20) \cdot 10^{-3};$$

$$B[c_0 \rightarrow \pi^+ K^+ K^-] = (1.78 \pm 0.05 \pm 0.23) \cdot 10^{-2};$$

For the decay mode  $c_0 \rightarrow f_0(980)f_0(980)$ , each  $f_0(980)$  can decay to either  $\pi^+ \pi^-$  or  $K^+ K^-$ , so it is necessary to divide the result in Table IV by a factor of 2 to obtain the branching fractions

$$B[(2S) \rightarrow c_0 \rightarrow f_0(980)f_0(980)] B[f_0(980) \rightarrow \pi^+ \pi^-] B[f_0(980) \rightarrow K^+ K^-] = (1.59 \pm 0.38^{+0.89}_{-0.72}) \cdot 10^{-5};$$

$$B[c_0 \rightarrow f_0(980)f_0(980)] B[f_0(980) \rightarrow \pi^+ \pi^-] B[f_0(980) \rightarrow K^+ K^-] = (1.73 \pm 0.42^{+0.96}_{-0.78}) \cdot 10^{-4};$$

Combining this result and that of Ref. [24], we can determine the ratio of the partial decay width of  $f_0(980)$  to those of  $\pi^+ \pi^-$  and  $KK$ :

$$\frac{\Gamma_{f_0(980) \rightarrow \pi^+ \pi^-}}{\Gamma_{f_0(980) \rightarrow K^+ K^-}} = \frac{(6.5 \pm 1.93) \cdot \frac{3}{2}}{(6.5 \pm 1.93) \cdot \frac{3}{2} + (1.59^{+0.95}_{-0.80}) \cdot 2} = 0.75^{+0.11}_{-0.12};$$

The numerical factors  $\frac{3}{2}$  and 2 take into account that (a) two-thirds of  $c_0$  decays are to  $\pi^+ \pi^-$  and one-third to  $0^+ 0^+$  and (b) there are equal numbers of decays to  $K^+ K^-$  and  $K^0 \bar{K}^0$ . Here the errors are the statistical and the systematic errors added in quadrature, and for the systematic error, the common parts related to the MDC tracking, kinematic fitting, efficiency of the photon ID, and the number of  $(2S)$  events cancel.

There is a strong  $f_0(980)f_0(2200)$  with a signal significance of 7.1 in the  $c_0 \rightarrow \pi^+ K^+ K^-$  decay. The mass and width of the  $f_0(2200)$  are optimized as  $M = 2170 \pm 20^{+10}_{-15}$  MeV/ $c^2$  and  $\Gamma = 220 \pm 60^{+40}_{-45}$  MeV/ $c^2$ , and

$$B[c_0 \rightarrow f_0(980)f_0(2200)] B[f_0(980) \rightarrow \pi^+ \pi^-] B[f_0(2200) \rightarrow K^+ K^-] = (8.42 \pm 1.16^{+1.65}_{-2.29}) \cdot 10^{-4};$$

Changing the spin-parity of the  $f_0(2200)$  in the fit or adding an additional resonance, shows that the spin-parity of the  $f_0(2200)$  is well determined and no additional resonance is needed in the  $f_0(2200)$  mass region. However, compared

to the nearby states  $f_0(2100)$  and  $f_2(2150)$ , its properties are still less well known [1], and more experimental data are needed.

Another significant decay mode to  $f_0(1370)f_0(1710)$  is also found with a significance of 6.5, where  $f_0(1370)$  decays to  $\pi^+\pi^-$  and  $f_0(1710)$  decays to  $K^+K^-$ . The fitted mass and width of the  $f_0(1710)$  are  $M = 1760_{-10}^{+15}$  MeV/ $c^2$  and  $\Gamma = 125_{-15}^{+25}$  MeV/ $c^2$ . The fitted mass is somewhat higher than the PDG value [1]. The spin 0 component can be separated from spin 2 clearly, and replacing  $f_0(1710)$  with either of the tensors  $f_2(1450)$  or  $f_2(1700)$  does not give a reasonable fit to the data. A fit to  $f_0(1370)$  gives a fitted mass of  $1265_{-35}^{+20}$  MeV/ $c^2$  and a width of  $350_{-60}^{+105}$  MeV/ $c^2$ . The corresponding branching fraction is

$$B[\pi^+\pi^- \rightarrow f_0(1370)f_0(1710)]B[f_0(1370) \rightarrow \pi^+\pi^-]B[f_0(1710) \rightarrow K^+K^-] = (7.12_{-1.68}^{+1.46}) \cdot 10^{-4}.$$

Besides the intermediate  $(\pi^+\pi^-)(K^+K^-)$  decay modes listed in Table I, we tried the following combinations in the fit:  $f_0(1370)f_0(1370)$ ,  $f_0(1370)f_0(1500)$ ,  $f_0(1500)f_0(1370)$ ,  $f_0(1500)f_0(1500)$ , and  $f_0(1500)f_0(1710)$ . None of them improved the log likelihood more than 5. So we didn't include these processes in the final solution of our fit and set upper limits at the 90% C.L.:

$$\begin{aligned} B[\pi^+\pi^- \rightarrow f_0(1370)f_0(1370)]B[f_0(1370) \rightarrow \pi^+\pi^-]B[f_0(1370) \rightarrow K^+K^-] &< 2.9 \cdot 10^{-4}; \\ B[\pi^+\pi^- \rightarrow f_0(1370)f_0(1500)]B[f_0(1370) \rightarrow \pi^+\pi^-]B[f_0(1500) \rightarrow K^+K^-] &< 1.8 \cdot 10^{-4}; \\ B[\pi^+\pi^- \rightarrow f_0(1500)f_0(1370)]B[f_0(1500) \rightarrow \pi^+\pi^-]B[f_0(1370) \rightarrow K^+K^-] &< 1.4 \cdot 10^{-4}; \\ B[\pi^+\pi^- \rightarrow f_0(1500)f_0(1500)]B[f_0(1500) \rightarrow \pi^+\pi^-]B[f_0(1500) \rightarrow K^+K^-] &< 0.55 \cdot 10^{-4}; \\ B[\pi^+\pi^- \rightarrow f_0(1500)f_0(1710)]B[f_0(1500) \rightarrow \pi^+\pi^-]B[f_0(1710) \rightarrow K^+K^-] &< 0.73 \cdot 10^{-4}; \end{aligned}$$

From the results of the fit, the branching fraction  $B[\pi^+\pi^- \rightarrow K(892)^0 K(892)^0 \rightarrow \pi^+\pi^- K^+K^-] = (8.09_{-1.99}^{+2.29}) \cdot 10^{-4}$  is obtained. Using the branching fraction of  $K(892)^0$  to the charged  $K$  mode, which is taken as  $\frac{2}{3}$ , we get

$$\begin{aligned} B[(2S) \rightarrow \pi^+\pi^- \rightarrow K(892)^0 K(892)^0] &= (1.68_{-0.40}^{+0.26}) \cdot 10^{-4}; \\ B[\pi^+\pi^- \rightarrow K(892)^0 K(892)^0] &= (1.82_{-0.45}^{+0.28}) \cdot 10^{-3}; \end{aligned}$$

The values obtained here are consistent with those in Ref. [4].

Most of the peak around a  $K$  mass  $1430$  MeV/ $c^2$  is fitted with  $K_0(1430)K_0(1430)$  and  $K_0(1430)K_2(1430) + c.c.$ , with only a small contribution from  $K_2(1430)K_2(1430)$ . The measured branching fractions are

$$\begin{aligned} B[\pi^+\pi^- \rightarrow K_0(1430)K_0(1430)^0 \rightarrow \pi^+\pi^- K^+K^-] &= (10.44_{-1.90}^{+1.57}) \cdot 10^{-4}; \\ B[\pi^+\pi^- \rightarrow K_0(1430)K_2(1430)^0 + c.c. \rightarrow \pi^+\pi^- K^+K^-] &= (8.49_{-1.99}^{+1.47}) \cdot 10^{-4}; \end{aligned}$$

A fit to  $K_0(1430)$  gives a fitted mass of  $1455_{-20}^{+15}$  MeV/ $c^2$  and a width of  $270_{-35}^{+45}$  MeV/ $c^2$ . The fitted number of  $K_2(1430)K_2(1430)$  events is about 11% of that of  $K_0(1430)K_0(1430)$ , and the signal significance of  $K_2(1430)K_2(1430)$  mode is about 3.3. These measurements are important for the study of  $\pi^+\pi^-$  decays, as well as those of  $K_0(1430)$  and  $K_2(1430)$ .

Using the results shown in Table IV and the branching fractions of  $K_1(1270) \rightarrow K(770)$  and  $K_1(1400) \rightarrow K(892)$  given by the PDG [1], we determine

$$\begin{aligned} B[\pi^+\pi^- \rightarrow K_1(1270)^+ K^- + c.c.] &= (6.66_{-1.51}^{+1.07}) \cdot 10^{-3}; \\ B[\pi^+\pi^- \rightarrow K_1(1400)^+ K^- + c.c.] &< 2.85 \cdot 10^{-3}; \end{aligned}$$

at the 90% C.L.. To accommodate this, a mixing angle of  $> 57^\circ$  is required. A Flavor-SU(3)-violating  $K_1(1270)K_1(1400)$  asymmetry is observed. The asymmetries with opposite character for  $(2S)$  and  $J=$  decays were also observed in the BES I data [25], where for  $(2S)$  data,  $< 29^\circ$  and for  $J=$  data  $> 48^\circ$ .

## V II. S U M M A R Y

In summary, a partial wave analysis on  $\pi^+\pi^- \rightarrow K^+K^-$  in  $(2S) \rightarrow \pi^+\pi^-$  decay is performed using a sample of 14 million  $(2S)$  events. From the two significant contributions to the  $\pi^+\pi^-$  decays from the channels  $f_0(980)f_0(980)$ ,  $f_0(980)f_0(2200)$ ,  $f_0(1370)f_0(1710)$ ,  $K(892)^0 K(892)^0$ ,  $K_0(1430)K_0(1430)$ ,  $K_0(1430)K_2(1430) + c.c.$  and  $K_1(1270)K_1(1400)$ . The mass and width of the  $f_0(1710)$  are determined to be  $1760_{-10}^{+15}$  MeV/ $c^2$  and  $125_{-15}^{+25}$  MeV/ $c^2$ , and those of the  $f_0(2200)$  are  $2170_{-15}^{+10}$  MeV/ $c^2$  and  $220_{-45}^{+60}$  MeV/ $c^2$ . Flavor-SU(3)-violating  $K_1(1270)K_1(1400)$  asymmetry is observed, with the mixing angle  $> 57^\circ$ .

## V III. ACKNOWLEDGMENT

We wish to thank Qiang Zhao for useful suggestions. The BES collaboration thanks the staff of BEPC for their hard efforts. This work is supported in part by the National Natural Science Foundation of China under contracts Nos. 10491300, 10225524, 10225525, 10425523, the Chinese Academy of Sciences under contract No. KJ 95T-03, the 100 Talents Program of CAS under Contract Nos. U-11, U-24, U-25, and the Knowledge Innovation Project of CAS under Contract Nos. U-602, U-34 (IHEP), the National Natural Science Foundation of China under Contract No. 10225522 (Tsinghua University), and the Department of Energy under Contract No. DE-FG 02-04ER 41291 (University of Hawaii).

- 
- [1] S. Eidelman et al: (Particle Data Group), Phys. Lett. B 592, 1 (2004).
  - [2] C. Amisler and F. E. Close, Phys. Rev. D 53, 295 (1996).
  - [3] Mark I Collaboration, W. M. Tanenbaum et al.; Phys. Rev. D 17, 1731 (1978).
  - [4] BES Collaboration, M. Ablikim et al.; Phys. Rev. D 70, 092003 (2004).
  - [5] BES Collaboration, J. Z. Bai et al.; Nucl. Instrum. Methods Phys. Res., Sect. A 458, 627 (2001).
  - [6] BES Collaboration, M. Ablikim et al.; physics/0503001.
  - [7] BES Collaboration, J. Z. Bai et al.; Phys. Rev. D 60, 072001 (1999).
  - [8] B. S. Zou and D. V. Bugg, Eur. Phys. J. A 16, 537 (2003).
  - [9] S. Dulat and B. S. Zou, hep-ph/0508087.
  - [10] S. M. Flatte, Phys. Lett. B 63, 224 (1976).
  - [11] B. S. Zou and D. V. Bugg, Phys. Rev. D 48, R3948 (1993).
  - [12] BES Collaboration, M. Ablikim et al.; Phys. Lett. B 598, 149 (2004).
  - [13] BES Collaboration, M. Ablikim et al.; Phys. Lett. B 607, 243 (2005).
  - [14] BES Collaboration, J. Z. Bai et al.; Phys. Rev. D 68, 052003 (2003).
  - [15] Crystal Barrel Collaboration, A. Abele et al.; Phys. Lett. B 468, 178 (1999).
  - [16] D. Aston et al.; Nucl. Phys. B 296, 493 (1988).
  - [17] W. G. Li, Hadron Spectroscopy, AIP Conf. Proc. No. 717 (AIP, Aachenburg, Germany, 2003), p. 495.
  - [18] See, for example, H. G. B. Lundell, S. Godfrey and B. Phelps, Phys. Rev. D 53, 3712 (1996); M. Suzuki, *ibid.*: 47, 1252 (1993), and references therein.
  - [19] E791 Collaboration, E. M. Aitala et al.; Phys. Rev. Lett. 86, 765 (2001).
  - [20] GAMMA Collaboration, R. Bellazzini et al.; Phys. Lett. B 467, 296 (1999).
  - [21] WA102 Collaboration, D. Barberis et al.; Phys. Lett. B 453, 316 (1999); 453, 325 (1999).
  - [22] X. H. Mo et al.; High Energy Phys. Nucl. Phys. 28, 455 (2004).
  - [23] CLEO Collaboration, S. B. Athar et al.; Phys. Rev. D 70, 112002 (2004).
  - [24] BES Collaboration, M. Ablikim et al.; Phys. Rev. D 70, 092002 (2004).
  - [25] BES Collaboration, J. Z. Bai et al.; Phys. Rev. Lett. 83, 1918 (1999).